

Document downloaded from:

<http://hdl.handle.net/10251/59988>

This paper must be cited as:

Borrell Tomás, MA.; Salvador Moya, MD.; García-Rocha, V.; Fernández, A.; Gómez, A.; López-López, E.; Moreno, R. (2014). ZrTiO<sub>4</sub> materials obtained by Spark Plasma Reaction Sintering. *Composites Part B: Engineering*. 56:330-335.  
doi:10.1016/j.compositesb.2013.08.046.



The final publication is available at

<http://dx.doi.org/10.1016/j.compositesb.2013.08.046>

Copyright Elsevier

Additional Information

**ZrTiO<sub>4</sub> materials obtained by Spark Plasma Reaction-Sintering**

Amparo Borrell\*<sup>1</sup>, María Dolores Salvador<sup>1</sup>, Victoria G. Rocha<sup>2</sup>, Adolfo Fernández<sup>2,3</sup>,  
Andrés Gómez<sup>4</sup>, Emilio López-López<sup>5</sup>, Rodrigo Moreno<sup>5</sup>

<sup>1</sup>Instituto de Tecnología de Materiales (ITM), Universitat Politècnica de València  
(UPV), Camino de Vera s/n, 46022 Valencia, Spain

<sup>2</sup>ITMA Materials Technology, Parque Tecnológico de Asturias, 33428 Llanera, Spain

<sup>3</sup>Centro de Investigación en Nanomateriales y Nanotecnología (CSIC-UO-PA), Parque  
Tecnológico de Asturias, 33428 Llanera, Spain

<sup>4</sup>Instituto de Ciencia de los Materiales (ICMUV), Parc Científic de la Universitat de  
València, Catedrático José Beltrán 2, 46980 Paterna, Valencia, Spain

<sup>5</sup>Instituto de Cerámica y Vidrio (ICV-CSIC), E-28049 Madrid, Spain

\*Corresponding author. Address: Instituto de Tecnología de Materiales (ITM),  
Universidad Politécnica de Valencia (UPV), Camino de Vera s/n, 46022 Valencia,  
Spain. Tel.: +34963877007; Fax: +34963877629.

E-mail address: aborrell@upvnet.upv.es (A. Borrell)

**Abstract**

Zirconium titanate (ZrTiO<sub>4</sub>), have many attractive properties such as high resistivity, high dielectric constant, high permittivity at microwave frequencies and excellent temperature stability for microwave properties. Zirconium titanate dense materials are proposed for many structural applications, but fully reacted and completely dense pieces are difficult to obtain by conventional routes. In this work, fully dense zirconium

titanate materials (~98%) were obtained at lower temperatures (1300-1400 °C) and short processing time by non-conventional technique; spark plasma-reaction sintering (SPRS). Homogeneous and stable starting powders mixture with the adequate composition was prepared from the raw materials: m-ZrO<sub>2</sub> (~0.3µm) and anatase-TiO<sub>2</sub> (~40nm). Dense materials were mechanically and microstructural characterized. The fracture strength was measured by biaxial testing, giving values of about 200 MPa.

**Keywords:** A. Ceramic-matrix composites (CMCs); B. Mechanical properties; B. Microstructure; E. Sintering

## 1. Introduction

Zirconium titanate (ZrTiO<sub>4</sub>) has been largely used in the field of electroceramics, as constituent of dielectric resonators and components for telecommunications [1-4]. More recently, the synthesis and structural characterization of zirconium titanate based materials have been studied focusing their high potential for applications requiring resistance to thermal shock, due to its anisotropy in the thermal expansion [5-8]. Synthesis of zirconium titanate powders can be made by different methods like co-precipitation [5,9] (800 - 1650 °C), sol-gel [10-12] (500 - 700 °C), mechanochemical processing [13] (room temperature), and solid-state reaction from ZrO<sub>2</sub> and TiO<sub>2</sub> powders [14-16].

Previous works reported the fabrication of single-phase ZrTiO<sub>4</sub> bulk materials by conventional sintering [7,16] from submicron-sized m-ZrO<sub>2</sub> and anatase-TiO<sub>2</sub> powders for structural applications. The process involved a two-steps schedule consisting in the slip casting and reaction sintering of ZrO<sub>2</sub> and TiO<sub>2</sub> to form ZrTiO<sub>4</sub> and the subsequent milling, isopressing and conventional sintering of those milled ZrTiO<sub>4</sub> powders.

However, this method has important drawbacks, the most important being, on one hand, that it is a multi-step process which needs long processing times with sintering cycles at 1500 °C and dwell times of up to 16 h and, on the other hand, that the maximum sintered density values attained are up to 94% of theoretical density (T.D.), much lower than desired for structural applications.

Accordingly, not only the green processing must be carefully controlled to improve the homogeneity of the phases but also the choice of the sintering method is crucial to obtain reaction sintered composites with improved properties. In this context fast sintering techniques such as Spark Plasma Sintering have demonstrated their suitability for producing sintered bodies with full density. This technique can work at heating rates of the order of hundreds of degrees per minute, reaching high temperatures in very short time, leading to dense materials after cycles of heating/cooling in the order of a few minutes [17-19]. These features allow achieving microstructures unattainable by other sintering techniques. The manufacture of alumina-aluminium titanate materials by slip casting and electrophoretic deposition (EPD) and further reaction sintering by SPS has been recently described [20,21], thus demonstrating the versatility of this sintering technology.

The main objective of this work was to produce dense single-phase zirconium titanate bulk materials with a direct, simple processing route. For such purpose, submicron-sized m-ZrO<sub>2</sub> and nano-sized anatase-TiO<sub>2</sub> powders were selected combining ~~for the first time~~ the freeze-drying of well dispersed suspensions to obtain homogeneous mixtures of the powders with a non-conventional sintering process such as spark plasma-reaction sintering (SPRS).

## 2. Experimental procedure

Commercial undoped m-ZrO<sub>2</sub> (TZ-0, Tosoh Tokyo, Japan) and anatase-TiO<sub>2</sub> (Aeroxide P25, Degussa, Germany) were used as starting powders to obtain ZrTiO<sub>4</sub> materials. Starting zirconia and anatase powders have average particle diameters of 300 nm and 40 nm, and specific surface areas of 14 m<sup>2</sup> g<sup>-1</sup> and 52 m<sup>2</sup> g<sup>-1</sup>, respectively. The approach used involves the preparation of a total solids loading suspension of 30 vol.%, with 15 vol.% of m-ZrO<sub>2</sub> and 15 vol.% of a-TiO<sub>2</sub>, using a poly(acrylic acid) based polyelectrolyte (Duramax D3005 Rohm and Haas, USA) as a dispersant to a total concentration of 5.2 wt.% on a dry solids basis. This high content of deflocculant is due to the nanometric size of titania that can be effectively dispersed with a concentration of 4 wt.% as demonstrated in previous work [22].

For the preparation of the materials, m-ZrO<sub>2</sub> powders were firstly added to the proper amount of distilled water containing the dispersant with the help of a high shear mixer (L2R, Silverson, Chesham, UK). Afterwards a-TiO<sub>2</sub> nanopowders were dispersed with the help of the high shear mixer and an ultrasonic probe (UP 400 S, Hielscher, Stuttgart, Germany). Sonication was performed using several cycles of 1 min, being the maximum sonication time of 8 min and a frequency of 24 kHz, since further sonication cycles led to reagglomeration. The final suspension was frozen in a liquid nitrogen bath and then dried in a freeze drier (Cryodos-50, Telstar, Spain) for 24 h.

Powders obtained were sieved using a 37 μm mesh nylon sieve and introduced into a 20-mm-diameter graphite die and sintered using a spark plasma sintering method (SPS), HP D25/1 apparatus (FCT Systeme GmbH, Rauenstein, Germany) at temperatures from 1300-1400 °C and 80 MPa of applied pressure to obtain fully sintered bulk materials. Tests were carried out under vacuum at a heating rate of 100 °C min<sup>-1</sup> with a 1 min of dwelling time at the maximum temperature.

Sintered density was determined by the Archimedes' method (ISO-3369) using deionized water.

The crystalline phases present were determined by X-ray diffraction. The obtained XRD patterns were analysed using the diffraction files of  $\text{ZrTiO}_4$  (PDF: 00-034-0415, density =  $5.08 \text{ g cm}^{-3}$ ) and  $\text{m-ZrO}_2$  (PDF: 00-037-1484, density =  $5.82 \text{ g cm}^{-3}$ ). Patterns for profile fitting using the Rietveld method [23] were obtained from a diffractometer (Bruker AXS-5005, SCSIE of the University of Valencia) using  $\text{Cu K}\alpha$  radiation. Compact pellets were used as samples and mounted in an appropriate sample holder. Patterns were collected with a scanning step of  $0.02^\circ$  between  $10$  and  $110^\circ$  in  $2\theta$  with a collection time of 10 s per step. Profile fittings were performed using the FULLPROF program [24].

The relative ratio between monoclinic zirconia and zirconium titanate was obtained from the profile fittings. Relative density of the sintered materials (% of T.D.) was evaluated considering that the final phases were Zirconium Titanate (ZT) and  $\text{m-ZrO}_2$  and taking into account the relative ratio of both phases. Error bars in the calculated densities are within the error of the measurements.

Sintered samples were longitudinally cut in half cylinders with a diamond saw. The samples were previously polished (Struers, model RotoPol-31) with diamond paste to  $0.25 \mu\text{m}$  roughness. Nanomechanical properties such as hardness and Young's modulus of samples were obtained by nanoindentation technique (Model G200, MTS Company, USA). To carry out indentations at very low depths, a brand new Berkovich diamond tip was used with radius less than 20 nm as certified by the manufacturing company. In order to ensure the quality of the tip throughout the work, pre- and post- calibration

procedures were performed for this indenter ensuring the correct calibration of its function area and correct machine compliance. The nanomechanical properties of the ZrTiO<sub>4</sub> ceramics were evaluated from the load-displacement nanoindentation data using the widely accepted Oliver and Pharr model [25].

The flexural strength was measured by biaxial testing using the equations of Kirstein and Woolley [26], Vitman and Pukh [27], and the standard specification ASTM F394-78. All tests were obtained at room temperature using a universal testing machine (Instron 856, MA, USA) with a cross-head displacement speed of 0.002 mm s<sup>-1</sup>. The fracture surface sections of the sintered samples have been observed using a field emission gun scanning electron microscope (FE-SEM, HITACHI S-4800, SCSIE of the University of Valencia).

### 3. Results and discussion

XRD patterns of the bulk ceramic ZrTiO<sub>4</sub> materials (ZT) sintered by spark plasma reaction-sintering (SPRS) at 1300, 1350 and 1400 °C are shown in Figure 1. They show that it is possible to obtain ZrTiO<sub>4</sub> materials at lower temperature than that used during normal solid-state reaction sintering [7,28]. Reflections at 2θ ~28° and 31° show the presence of residual m-ZrO<sub>2</sub>, whereas it is not possible to observe characteristic peaks of TiO<sub>2</sub>.

It must be stressed that ZrO<sub>2</sub>/TiO<sub>2</sub> ratio used to prepare green compacts was calculated to obtain single-phase zirconium titanate materials [7,16].

If ZT phase obtained would be stoichiometric (i.e., ZrTiO<sub>4</sub>), the presence of residual m-ZrO<sub>2</sub> should be accompanied by residual TiO<sub>2</sub>. However, we have not observed TiO<sub>2</sub> XRD peaks in the diffraction pattern, which could be attributed to its low relative

intensity.

Nevertheless, investigations in the phase diagram of  $\text{ZrO}_2\text{-TiO}_2$  show the existence of a disordered  $\text{Zr}_{1-x}\text{Ti}_{1+x}\text{O}_4$  at temperatures above ie. 1150 °C. The presence of m- $\text{ZrO}_2$  is compatible, then, with a ZT phase with a Ti/Zr ratio  $(1+x)/(1-x)$  greater than 1. The situation can be, indeed, more complicated due to the significant solubility of Ti in  $\text{ZrO}_2$  at such temperatures.

In order to determine the m- $\text{ZrO}_2$  content and the Ti and Zr stoichiometry in the ZT phase, we have performed profile fittings of XRD patterns of the samples. Summarized in Table 1 are the main data obtained for the samples prepared at 1300, 1350 and 1400 °C. The fits were performed considering a mixture of  $\text{Zr}_{1-x}\text{Ti}_{1+x}\text{O}_4$  and m- $\text{ZrO}_2$  phases. Although we have indicated above the significant solubility of Ti in  $\text{ZrO}_2$  at high temperatures, the low intensity of the zirconia reflections precludes the evaluation of the Ti present in the m- $\text{ZrO}_2$  by such analysis. A pseudo-Voigt peak-shape function was used. In the final runs, the usual profile parameters (scale factors, background coefficients, zero-points, half-width, pseudo-Voigt and asymmetry parameters for the peak-shape) were refined. Cell parameters, atomic positions and  $x$  were refined for  $\text{Zr}_{1-x}\text{Ti}_{1+x}\text{O}_4$ . However, for m- $\text{ZrO}_2$ , due to the low intensity of its reflections, only cell parameters were refined. Isotropic thermal parameters were set at 0.5 and 0.9 Å<sup>2</sup> for metal and oxygen atoms, respectively, and an overall thermal parameter was also refined for each phase.

Cell parameters for ZT showed in Table 1 are close with data reported previously for  $\text{ZrTiO}_4$  air quenched from the sintering temperature [7], which indicate that the cooling rate of SPS is very high.

We have made the refinements considering a disordered ZT phase. Such assumption is reasonable taking into account that we have not observed the characteristic

superstructure reflections of the ordered phase. In addition,  $b$  cell parameter, a well-known indicator of the state of ordering in ZT phase [15], have values typical of disordered phases in all the samples.

The calculated m-ZrO<sub>2</sub> content is around 9% for samples prepared at 1300 and 1350 °C, and decreases to 3.9% for the samples prepared at 1400 °C. On the other hand, the  $x$  parameter, that measures the non-stoichiometry in the ZT phase, is 0.17 at 1300, 0.15 at 1350 °C, and decreases to 0.11 at 1400 °C. The evolution of both parameters, m-ZrO<sub>2</sub> content and  $x$ , are in good accordance.

It was reported in a previous work [7] that a liquid phase was developed in single-phase ZrTiO<sub>4</sub> materials for sintering temperatures higher than 1500 °C, limiting the maximum treatment temperature. Moreover, as the complete reaction of formation of ZrTiO<sub>4</sub> occurred before shrinkage of the compact (<1450 °C) during the reaction sintering process and the final densities were extremely low ( $\approx$  84% T.D.). To obtain single-phase ZrTiO<sub>4</sub> materials with higher density by a conventional sintering process it was necessary to prepare green bodies by slip casting that were sintered at 1500 °C and further attrition milled and sieved, but after this complex multi-step process final densities of about 94% of T.D. were obtained [16], far from the near to full density required for some structural applications.

Relative densities of the all specimens sintered by SPRS at different temperatures (1300-1400 °C) were calculated on the basis of a complete reaction, but the deviation due to the presence of unreacted zirconia is inside the error ( $\pm$ 1.0 % T.D.). The relative density values of the material obtained at 1300 °C, 1350 °C and 1400 °C are approximately 96.5, 97.7 and 98.2 % T.D., respectively. The sample sintered at 1400 °C

shows a very high value compared with reported by López-López et al. [16]. These authors reported that the maximum relative density of  $ZrTiO_4$  materials obtained by conventional sintering at 1500 °C during 16 h as maximum dwell time, is approximately 94% T.D, which is too low for being used in structural applications. Moreover, materials treated at 1500 °C during 4 and 8 h showed high open porosity values (19 and 13%, respectively), which correspond to initial sintering stages [16]. Then, the use of non-conventional sintering techniques in this study, such as SPRS, which applies pressure and temperature simultaneously, is a good solution for complete densification without porosity of low sinterability materials such as zirconium titanate.

The improved densification of the obtained composites is probably due to the peculiar heating mode in SPRS that potentially induces a thermal effect related to the presence of an electrical field. The presence of an electrical field can potentially affect surface phenomena by modifying the grain boundary energy and interface kinetics [29]. This could lead to a delay in the grain growth process and enhance sinterability.

Even in poorly conducting materials like alumina, the presence of an electric field has been shown to drastically enhance the diffusion of species contributing to densification (change in the rate-controlling diffusion mechanism) [30]. The surface diffusion is probably enhanced from the earlier stages of the sintering cycle leading to a faster formation of the sintering necks. The high heating rates applied in SPRS allow reaching quickly a temperature range where the densification process is favoured and kinetically separated from grain growth. The impurities or added second phases could also play an important role.

The activation energy values for high sintering temperatures and heating rates suggests

the contribution of additional mechanisms most probably related to the presence of the electric field and to the increase of the electrical conductivity of the samples at high temperature.

FE-SEM micrographs of fracture surface of  $\text{ZrTiO}_4$  materials obtained by SPRS at different temperatures are shown in Figure 2. As it can be observed, sintered specimens with polyhedral grains are obtained in all cases. Residual porosity can be detected in the sample sintered at the lowest temperature. As it could be expected, the average grain size increases with temperature and it can be roughly estimated to be around 0.4, 0.6, and 0.8  $\mu\text{m}$  for 1300, 1350, and 1400  $^\circ\text{C}$ , respectively. Grain size distribution is also coarser as sintering temperature increased.

The presence of nanometric particles randomly distributed along the samples, and especially at grain boundaries and triple points can be also detected. It has commented before (experimental part) that m- $\text{ZrO}_2$  and  $\text{TiO}_2$  used to process these materials have grain size of 300 and 40 nm, respectively. X-ray pattern do not show the presence of titania without reacting and the grain size of m- $\text{ZrO}_2$  used is bigger than the size of the nanoparticles observed in the microstructure. Therefore, it is thought that these nanoparticles have been formed during cooling by precipitation as a result of the lower solubility of m- $\text{ZrO}_2$  in  $\text{ZrTiO}_4$  [31].

Microstructures of all specimens show equiaxial grains and only residual microcracks. Young's modulus values of these materials (Table 2) are in agreement with data previously reported [16] for a fully dense single phase zirconium titanate material ( $161 \pm 4$  GPa). In addition, grain size of  $\text{ZrTiO}_4$  in all specimens ( $\sim 0.4\text{-}0.8$   $\mu\text{m}$ ) (Fig. 2) is

much lower than that reported by López-López et al. for single phase zirconium titanate materials processed by conventional sintering ( $\sim 4\text{-}8\ \mu\text{m}$ ) [16], which do not show microcracking in their microstructures. Therefore, the isolated residual microcracks observed in the materials of Fig. 2, could be originated during the fracture process.

The fracture mode observed in these materials is predominantly intergranular. Only isolated transgranular fractures can be observed that could correspond to the largest grains. A change in the fracture mode of  $\text{ZrTiO}_4$  as a function of the grain size has been previously reported in zirconium titanate-zirconia composite materials [28].

The simultaneous applications of current and pressure during non-conventional sintering by SPRS technique are beneficial to obtain completely reacted and homogeneous sintered materials. Pressure assisted sintering methods increase the driving force for densification. On the other hand, electrical current activates the particles surface improving their reactivity and therefore, favouring zirconium titanate formation. In Table 2 they are summarized the mechanical properties determined on  $\text{ZrTiO}_4$  sintered materials.

There are no data reported in the literature regarding fracture strength of  $\text{ZrTiO}_4$  to compare these results. Regarding fracture strength the highest value was obtained for the material sintered at  $1350\ \text{°C}$ . This material shows a good balance between densification and grain growth inhibition. Its porosity is lower than 3% and the average grain size is lower than  $1\ \mu\text{m}$ . The further improvement of density when the material is sintered at  $1400\ \text{°C}$  is accompanied by slightly grain growth reducing their mechanical properties, fracture strength and hardness. Young's modulus values are very similar for

all materials and are in agreement with published data obtained by nanoindentation and the Impulse Excitation Technique on conventionally sintered  $\text{ZrTiO}_4$  materials [16].

The evolution of the hardness (H) and Young's modulus (E) with penetration depth for the three studied materials is plotted in Figure 3. A common trend can be clearly detected in the behaviour of H and E values as a function of penetration depth. Hardness and Young's modulus values decrease when penetration depth increases. The slope of the curves is very slow and they finally stabilize in all experimented penetration depths. Dispersion of H and E are very large for the initial 200 nm of penetration depth. This fact could be due to the implicit experimental variability of factors such as tip-sample interactions, sample roughness and tip rounding [32].

The slightly decrease of H with penetration depth could be due to the indentation size effect [33]. Concerning elastic modulus, the obtained values show a little decrease according to the penetration depth. This may be due to the residual stresses in the material obtained by SPRS process [34]. SPRS introduces stresses that concentrate at grain boundaries and inhibit extensive crack growth, resulting in good mechanical properties for their use as structural materials. However, elastic properties are slightly affected probably due to microcracking under the indentation tip due to the residual stresses present in this material as consequence of the thermal expansion anisotropy of  $\text{ZrTiO}_4$  and SPRS process [34]. In addition, the higher is the depth of penetration, the more likely is that residual porosity and grain boundaries can affect H and E values.

#### 4. Conclusions

In conclusion, in situ zirconium titanate bulk ceramic materials were successfully

obtained from submicron-sized zirconia and nano-sized titania powders and consolidated by SPRS at temperatures ranging from 1300 to 1400 °C with a dwell time of 1-min. To the best of our knowledge there is no literature reporting any study by spark plasma sintering of single-phase  $\text{ZrTiO}_4$  materials. Therefore, although a residual unreacted zirconia fraction is still detected, the fabrication of nearly pure zirconium titanate by SPRS is reported in this work for the first time. Further readjustments in the starting mixture could easily lead to the pure single phase, and a major presence of this phase can contribute to enhance the final properties.

The density achieved is very high in comparison to conventional sintering processes (~98% versus 94% of T.D.), and the  $\text{ZrTiO}_4$  average grain size ranges in materials treated at different temperatures are around 0.4 to 1.0  $\mu\text{m}$ .

Young's modulus values are in good agreement with the value published previously in the literature, which was evaluated from experimental data of single phase  $\text{ZrTiO}_4$  materials with different degrees of porosity determined by impulse excitation technique. Fracture strength and hardness values for  $\text{ZrTiO}_4$  bulk materials are reported for the first time.

### **Acknowledgements**

This study has been supported by the Spanish Ministry of Science and Innovation MAT2009-14144-C03-02, MAT2012-38364-C03-02 and MAT2012-31090. A. Borrell, acknowledges the Spanish Ministry of Science and Innovation for her *Juan de la Cierva* contract (JCI-2011-10498) and the Generalitat Valenciana for the BEST/2012/302 grant and the financial support for ACOMP/2012/166.

### **References**

- [1] Park Y, Kim Y. Influence on cooling rate on the physical properties of tin modified zirconium titanate. *J Mater Sci Lett* 1996;15:853-5.
- [2] Wolfram G, Göbel HE. Existence range, structural and dielectric properties of  $Zr_xTi_ySn_zO_4$  ceramics ( $X + Y + Z = 2$ ). *Mater Res Bull* 1981;16:1455-63.
- [3] Bianco A, Gusmano G, Freer R, Smith P. Zirconium titanate microwave dielectrics prepared via polymeric precursor route. *J Eur Ceram Soc* 1999;19:959-63.
- [4] Hirano S, Hayashi T, Hattori A. Chemical processing and microwave characteristic of  $(Zr,Sn)TiO_4$  microwave dielectrics. *J Am Ceram Soc* 1991;74:1320-4.
- [5] Kudesia R, Snyder RL, Condrate RD, McHale AE. Structural Study of  $Zr_{0.8}Sn_{0.2}TiO_4$ . *J Phys Chem Solids* 1993;54:671-84.
- [6] Ikawa H, Iwai A, Hiruta K, Shimojima H, Urabe K, Udagawa S. Phase transformation and thermal expansion of zirconium and hafnium titanates and their solid solutions. *J Am Ceram Soc* 1988;71:120-7.
- [7] López-López E, Baudín C, Moreno R, Santacruz I, León-Reina L, Aranda MAG. Structural characterization of bulk  $ZrTiO_4$  and its potential for thermal shock applications. *J Eur Ceram Soc* 2012;32:299-306.
- [8] López-López E, Baudín C, Moreno R. Thermal expansion of zirconia-zirconium titanate materials obtained by slip casting of mixtures of Y-TZP- $TiO_2$ . *J Eur Ceram Soc* 2009;29:3219-25.
- [9] Krebs MA, Condrate RA. A raman spectral characterization of various crystalline mixtures in the  $ZrO_2$ - $TiO_2$  and  $HfO_2$ - $TiO_2$  systems. *J Mater Sci Lett* 1988;7:1327-30.
- [10] Sahn EL, Aranda MAG, Farfan-Torres EM, Gottifredi JC, Martinez-Lara M, Bruque S. Zirconium titanate from sol-gel synthesis: Thermal decomposition and quantitative phase analysis. *J Solid State Chem* 1998;139:225-32.
- [11] Bhattacharya AK, Mallick KK, Hartridge A, Woodhead JL. Sol-gel preparation,

structure and thermal stability of crystalline zirconium titanate microspheres. *J Mater Sci* 1996;31:267-71.

[12] Navio JA, Marchena FJ, Macias M, Sanchez-Soto PJ, Pichat P. Formation of zirconium titanate powder from a sol-gel prepared reactive precursor. *J Mater Sci* 1992;27:2463-7.

[13] Gajovic A, Furic K, Music S, Djerdj I, Tonejc A, Tonejc AM, Su D, Schlogl R. Mechanism of  $ZrTiO_4$  synthesis by mechanochemical processing of  $TiO_2$  and  $ZrO_2$ . *J Am Ceram Soc* 2006;89:2196-205.

[14] McHale AE, Roth RS. Low-temperature phase relationships in the system  $ZrO_2$ - $TiO_2$ . *J Am Ceram Soc* 1986;69:827-32.

[15] Troitzsch U, Ellis DJ. The  $ZrO_2$ - $TiO_2$  phase diagram. *J Mater Sci* 2005;40:4571-7.

[16] López-López E, Erauw JP, Moreno R, Baudín C, Cambier F. Elastic behaviour of zirconium titanate bulk material at room and high temperature. *J Eur Ceram Soc* 2012;32:4083-9.

[17] Munir ZA, Anselmi-Tamburini U, Ohyanagi M. The effect of electric field and pressure on the synthesis and consolidation of materials: a review of the spark plasma sintering method. *J Mater Sci* 2006;41:763-77.

[18] Joanna RG, Antonios Z. Sintering activation by external electrical field. *Mater Sci Eng A* 2000;287:171-7.

[19] Yucheng W, Zhengyi F. Study of temperature field in spark plasma sintering. *Mater Sci Eng B* 2002;90:34-7.

[20] Borrell A, Salvador MD, Rocha VG, Fernández A, Molina T, Moreno R. Enhanced properties of alumina-aluminium titanate composites obtained by spark plasma reaction-sintering of slip cast green bodies. *Comp Part B* 2013;47:255-9.

[21] Borrell A, Salvador MD, Rocha VG, Fernández A, Molina T, Moreno R. EPD and

Spark Plasma Sintering of bimodal alumina/titania concentrated suspensions. *J Alloys*

*Compd* doi: 10.1016/j.jallcom.2013.04.175

[22] Vicent M, Sánchez E, Santacruz I, Moreno R. Dispersion of TiO<sub>2</sub> nanopowders to obtain homogeneous nanostructured granules by spray-drying. *J Eur Ceram Soc* 2011;31:1413-9.

[23] Rietveld HM. A profile refinement method for nuclear and magnetic structures. *J Appl Crystallogr* 1969;2:65-71.

[24] Rodriguez-Carvajal J. FullProf Program, Collected Abstracts of Powder Diffraction Meeting, Toulouse, France, 1990, 127-128.

[25] Oliver WC, Pharr GM. An improved technique for determining hardness and elastic modulus using load and displacement sensing indentation experiments. *J Mater Res* 1992;7:1564-83.

[26] Kirstein AF, Woolley RM. Symmetrical bending of thin circular elastic plates on equally spaced point supports. *J Res Natl Bur Stand C* 1967;71:1-10.

[27] Vitman FF, Pukh VP. A method for determining the strength of sheet glass. *Zavod Lab* 1963;29:863-7.

[28] López-López E, Sanjuán ML, Moreno R, Baudín C. Phase Evolution in Reaction Sintered Zirconium Titanate Based Materials. *J Eur Ceram Soc* 2010;30:981-91.

[29] Ghosh S, Chokshi AH, Lee P, Raj R. A huge effect of weak dc electrical fields on grain growth in zirconia. *J Am Ceram Soc* 2009;92:1856-9.

[30] Yang D, Conrad H. Plastic deformation of fine-grained Al<sub>2</sub>O<sub>3</sub> in the presence of an electric field. *Scripta Mater* 1999;41:397-401.

[31] López-López E, Moreno R, Baudín C. Titanato de circonio: estabilidad termodinámica y expansión térmica. *Bol Soc Esp Ceram Vidrio* 2011;50:169-78.

[32] Botero CA, Jiménez-Piqué E, Baudín C, Salán N, Llanes L. Nanoindentation of

Al<sub>2</sub>O<sub>3</sub>/Al<sub>2</sub>TiO<sub>5</sub> composites: Small-scale mechanical properties of Al<sub>2</sub>TiO<sub>5</sub> as reinforcement phase. *J Eur Ceram Soc* 2012;32:3723-31.

[33] Botero CA, Jiménez-Piqué E, Seuba J, Kulkarni T, Sarin VK, Llanes L. Mechanical behaviour of 3Al<sub>2</sub>O<sub>3</sub>·2SiO<sub>2</sub> films under nanoindentation. *Acta Mater* 2012;60:5889-99.

[34] Alvarez-Clemares I, Borrell A, Agouram S, Torrecillas R, Fernandez A. Microstructure and mechanical effects of spark plasma sintering in alumina monolithic ceramics. *Scripta Mater* 2013;68:603-6.

ACCEPTED MANUSCRIPT

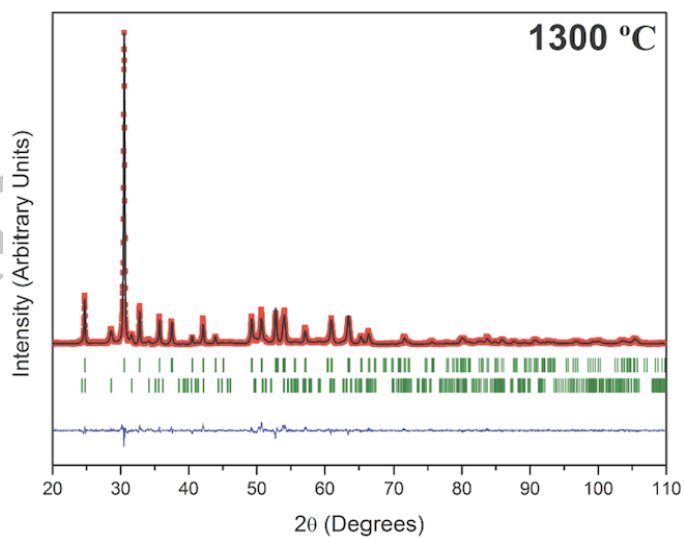
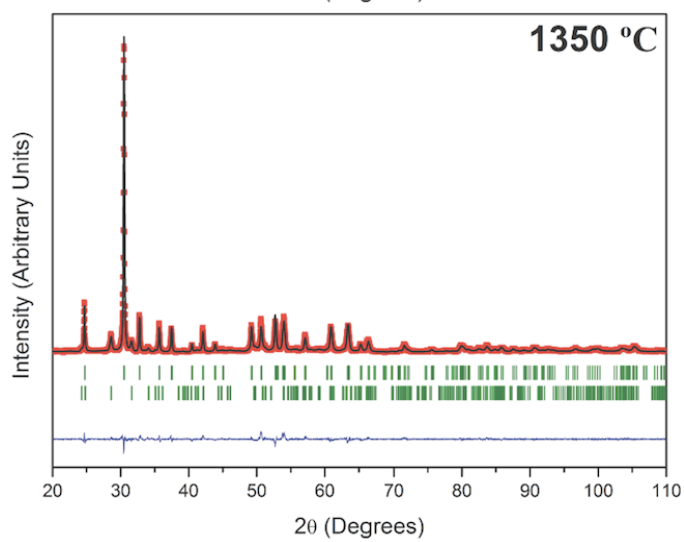
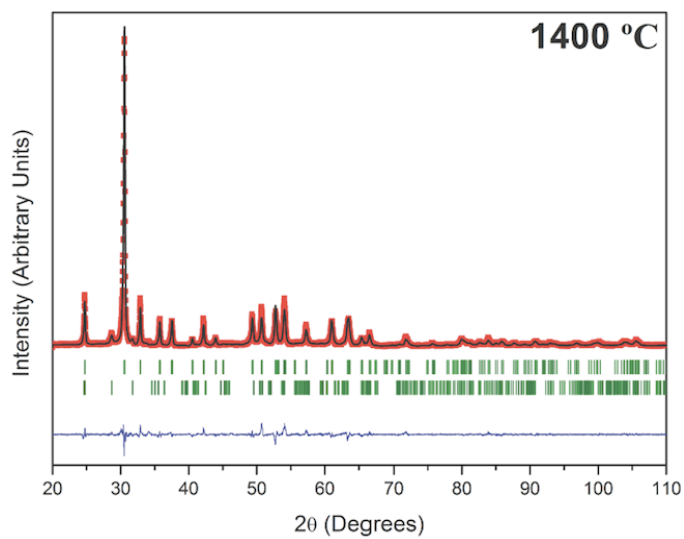
**Figure captions:**

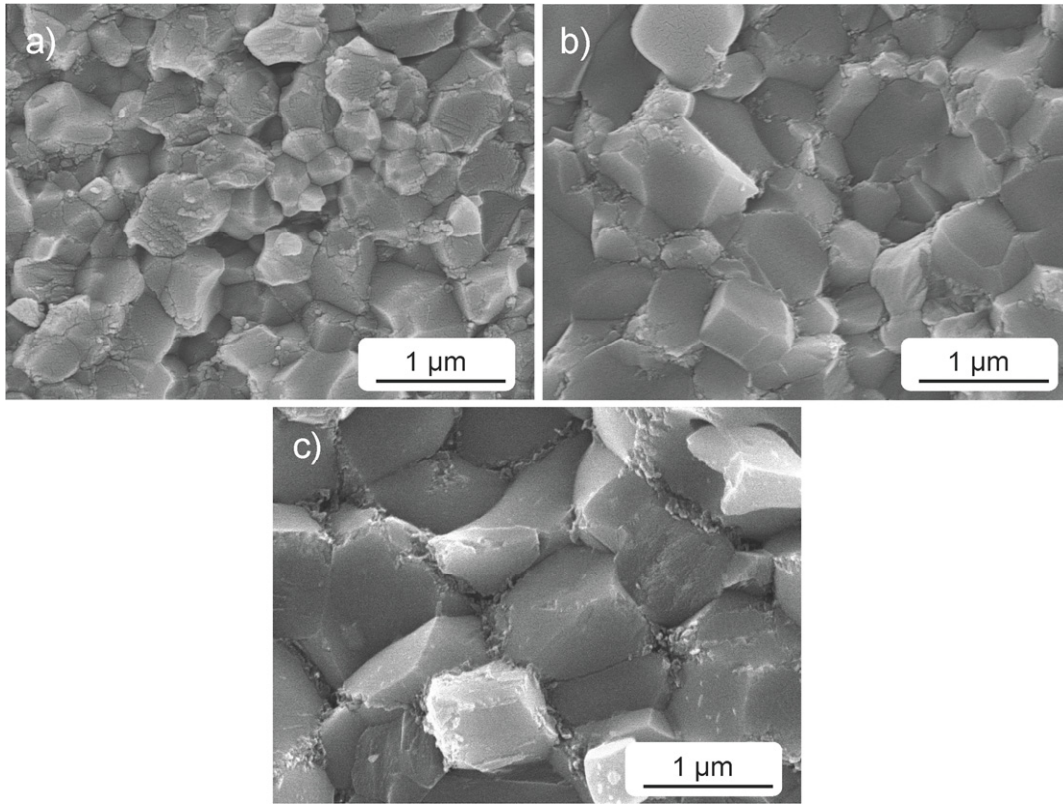
Figure 1. Observed (dotted) and calculated (solid) X-ray diffraction profiles for  $\text{ZrTiO}_4$  bulk ceramic materials sintered by SPRS at 1300 °C, 1350 °C and 1400 °C. Tic marks below the diffractograms represent the allowed Bragg reflections. The residuals lines are located at the bottom of the figures.

Figure 2. FE-SEM micrographs of fracture surface of  $\text{ZrTiO}_4$  materials obtained by SPRS at different temperatures: a) 1300 °C, b) 1350 °C and c) 1400 °C.

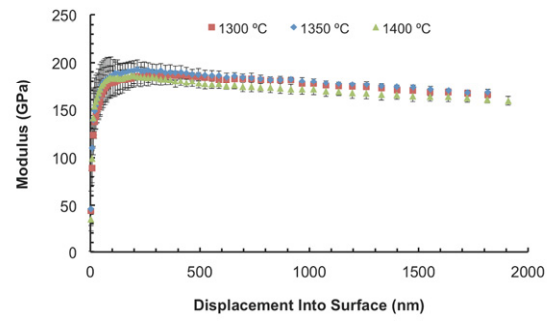
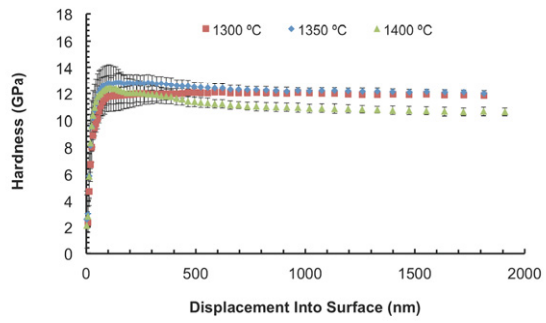
Figure 3. Hardness and Young's modulus evolution of  $\text{ZrTiO}_4$  materials with penetration depth.

ACCEPTED MANUSCRIPT





ACCEPTED MANUSCRIPT



ACCEPTED MANUSCRIPT

		1300 °C	1350 °C	1400 °C
<b>Zr<sub>1-x</sub>Ti<sub>1+x</sub>O<sub>4</sub></b>	<b><i>a</i></b>	4.79101 (9)	4.7965 (7)	4.7974 (12)
	<b><i>b</i></b>	5.4630 (9)	5.4638 (7)	5.4479 (11)
	<b><i>c</i></b>	5.0287 (8)	5.0316 (6)	5.0241 (10)
	<b><i>V</i></b>	131.62 (4)	131.86 (3)	131.31 (5)
	<b><i>M<sub>y</sub></i></b>	0.2006 (6)	0.2009 (5)	0.2020 (7)
	<b><i>O<sub>x</sub></i></b>	0.2668 (23)	0.2692 (19)	0.270 (3)
	<b><i>O<sub>y</sub></i></b>	0.3945 (19)	0.3936 (16)	0.3912 (22)
	<b><i>O<sub>z</sub></i></b>	0.4321 (20)	0.4347 (16)	0.4357 (23)
	<b><i>x</i></b>	0.17 (5)	0.15 (4)	0.11 (9)
	<b>%</b>	91 (5)	91 (4)	96 (6)
	<b><i>R<sub>B</sub></i></b>	4.83	4.84	4.48
<b>ZrO<sub>2</sub></b>	<b><i>a</i></b>	5.102 (5)	5.100 (4)	5.179 (7)
	<b><i>b</i></b>	5.112 (5)	5.113 (4)	5.053 (7)
	<b><i>c</i></b>	5.309 (5)	5.316 (3)	5.247 (7)
	<b><i>β</i></b>	98.42 (5)	98.44 (3)	98.66 (9)
	<b><i>V</i></b>	137.00 (22)	137.11 (15)	135.7 (3)
	<b>%</b>	8.8 (1.2)	9.0 (1.0)	3.9 (0.5)
	<b><i>R<sub>B</sub></i></b>	7.54	6.64	9.89
	<b><i>R<sub>p</sub></i></b>	16.8	15.6	16.5
	<b><i>R<sub>wp</sub></i></b>	18.7	17.4	18.4
	<b><i>χ<sup>2</sup></i></b>	1.87	1.64	2.30

Table 1. Selected data from X-ray powder diffraction studies of Zr<sub>1-x</sub>Ti<sub>1+x</sub>O<sub>4</sub> samples prepared at 1300, 1350 and 1400 °C by SPRS.

Zr<sub>1-x</sub>Ti<sub>1+x</sub>O<sub>4</sub>: Space group Pbcn. m-ZrO<sub>2</sub>: Space group P2<sub>1</sub>/c. *R<sub>p</sub>* and *R<sub>wp</sub>* are conventional (background corrected) peak only Rietveld profile and weighted profile residuals. *R<sub>B</sub>* is the integrated intensity residual, and *χ<sup>2</sup>* the square of the goodness-of-fit.

Sintering temperature (°C)	$\sigma_f$ (MPa)	H (GPa)	E (GPa)
1300	194 $\pm$ 2	12.0 $\pm$ 0.1	173 $\pm$ 1
1350	227 $\pm$ 3	12.2 $\pm$ 0.2	176 $\pm$ 2
1400	205 $\pm$ 3	10.8 $\pm$ 0.3	167 $\pm$ 5

Table 2. Fracture strength ( $\sigma_f$ ), hardness (H) and Young's modulus (E) values of the ZrTiO<sub>4</sub> materials obtained by SPRS at different temperatures.